Eroglu, S., et al., 2021, The impact of postdepositional alteration on iron- and molybdenum-based redox proxies: Geology, v. 49, https://doi.org/10.1130/G49291.1

GSA SUPPLEMENTAL MATERIAL

"The impact of postdepositional alteration on iron- and molybdenum-based redox proxies"

S. Eroglu, F. Scholz, R. Salvatteci, C. Siebert, R. Schneider, M. Frank

1. Scientific background

1.1. Fe-based redox proxies

Threshold values between different Fe speciation ratios and diagnostic "marine redox" fields have been defined based on calibrations in modern marine depositional settings (Fig. 1 A) (Poulton and Canfield, 2011; Raiswell et al., 2018). As an example, Fe_{HR}/Fe_T ratios <0.22 are applied to characterize sediments deposited under oxic conditions whereas ratios from 0.22 to 0.38 (Lyons and Severmann, 2006; Lyons et al., 2003; Poulton and Canfield, 2005; Scholz, 2018) can be indicative for possibly anoxic (either ferruginous or euxinic) and for ratios >0.38 diagnostic for Fe mobilization and accumulation under ferruginous (anoxic, non-sulfidic and Fe-rich) or euxinic (anoxic and sulfidic) seawater conditions (Poulton and Canfield, 2011; Raiswell and Canfield, 1998). The Fe_{py}/Fe_{HR} ratio represents the extent of pyritization (Berner, 1970) indicating sulfurization of reactive Fe minerals, in particular of Fe-(oxyhydr)oxides and -carbonates. High Fe_{py}/Fe_{HR} ratios >0.80 are applied as indicators of euxinic conditions in the bottom waters during deposition (Anderson and Raiswell, 2004; Canfield et al., 2008; Poulton et al., 2004).

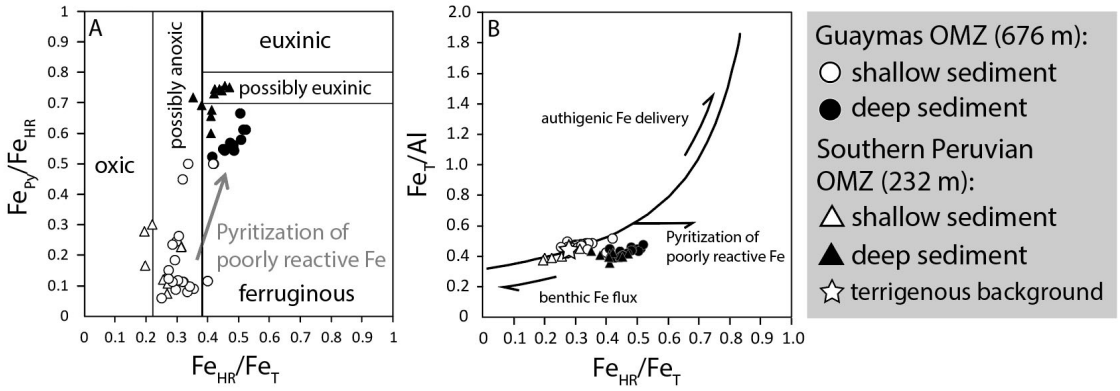

Figure S1: Fe speciation ratios of shallow and deep sediments from the Guaymas and southern Peruvian OMZs. Pyritization of poorly reactive silicate Fe during burial causes an increase in highly reactive Fe (FE_{HR}) over total Fe (Fe_T). A) Cross plot of Fe_{Py}/Fe_{HR} versus Fe_{HR}/Fe_T showing fields that are indicative for oxic, anoxic-ferruginous and anoxic-sulfidic conditions (März et al., 2008; Poulton and Canfield, 2011; Raiswell et al., 2001). The transitional area can be indicative to either oxic or anoxic conditions. B) Cross plot of Fe_T/Al versus Fe_{HR}/Fe_T showing the trend line that is indicative for a net Fe enrichment/depletion of reactive Fe due to authigenic Fe delivery/sedimentary Fe release. Concept and data interpretation explained in detail in Scholz (2018). The open star represents terrigenous background sedimentation on the Peruvian margin (Scholz, 2018).

A combination of Fe_{HR}/Fe_T and total Fe over aluminum (Fe_T/Al) can be used to identify redox-dependent sedimentary Fe release or trapping (Lyons et al., 2003; Scholz, 2018). Importantly, the shape of the trend line and its position within the Fe_T/Al versus Fe_{HR}/Fe_T space solely depends on the initial Fe_T/Al and Fe_{HR}/Fe_T (corresponding to the terrigenous background sedimentation) prior to the gain or loss of

reactive Fe due to Fe precipitation from the water column and sedimentary Fe release. Conversely, any change in Fe_{HR}/Fe_T without equivalent change in Fe_T/Al has to be related to a transfer of Fe from the unreactive to the reactive Fe pool (e.g., through pyritization of poorly reactive or unreactive silicate Fe) or vice versa (e.g, through precipitation of authigenic silicate minerals) without net gain or loss of Fe relative to Al.

1.2. Mo-based redox proxies

The different fractionation mechanisms in oxic and sulfidic settings and differences in supply mechanisms and diagenetic cycling result in a wide range of δ^{98}Mo signatures (Fig. 2 A) that have been observed in open-marine anoxic settings in previous studies (Eroglu et al., 2020; McManus et al., 2006; Poulson-Brucker et al., 2009; Poulson et al., 2006; Siebert et al., 2006). These studies attributed light Mo isotope compositions to adsorption to Mn-Fe oxides (Poulson et al., 2006; Siebert et al., 2006) whereas heavier Mo isotope compositions were linked to fractionation processes associated with sedimentary sulfide formation (Poulson-Brucker et al., 2009; Poulson et al., 2006; Siebert et al., 2006). In semi-restricted euxinic basins (e.g. the Black Sea) this process is quantitative resulting in isotopically heavy δ^{98}Mo signatures close to open-ocean seawater values (Arnold et al., 2004; Barling et al., 2001). Molybdenum isotope data from anoxic open marine settings show an average value near +1.6 ‰ (Fig. 2 A). However, a recent study has shown that the delivery mode of Mo significantly influences its isotope signature by either shifting δ^{98}Mo to lighter signatures (delivery via particles) or leading to heavier signatures close to seawater (delivery via diffusion) (Eroglu et al., 2020).

Thio-molybdate is particle reactive and readily scavenged from the water column by protonated particles into sulfidic sediment surfaces, either by irreversible incorporation into Fe-Mo-sulfides (Helz et al., 2014; Helz et al., 1996) or by adsorption onto sulfurized organic matter (Chappaz et al., 2014; Dahl et al., 2017; Helz et al., 1996; Tribovillard et al., 2004; Wagner et al., 2017), thereby retaining and accumulating Mo in the sediment (Bostick et al., 2003; Dellwig et al., 2002; Huerta-Diaz and Morse, 1992; Raiswell and Plant, 1980). Molybdenum is highly enriched in settings where the water column is sulfidic, although settings with sulfidic porewater or intermittently/permanently euxinic conditions show a high variability (Fig. 2 B) (Scott and Lyons, 2012). The deep sediments from the Guaymas OMZ show relatively low Mo enrichments, supporting the observation of heavy Mo isotope signatures and diffusive Mo supply from bottom water. The deep sediments from the southern Peruvian margin show low to moderate Mo enrichments, which can be best explained by a combination of Mo delivery via particles and fixation in sulfidic sediments (Eroglu et al., 2020). This is confirmed by the relatively light Mo isotope signature of these samples.

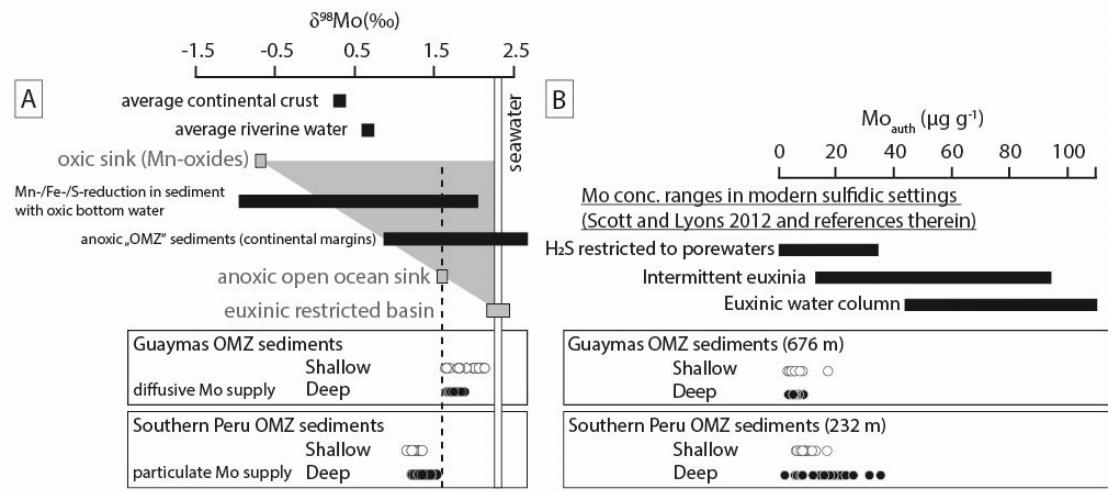

Figure S2: (A) Overview of the Mo isotope redox proxy with typical isotopic ranges (black bars) measured in different redox environments (after Poulson-Brucker et al. (2009), Poulson-Brucker et al. (2012) and Siebert et al. (2003)). Grey boxes indicate isotopic "end-members". The Mo supply mechanisms are an important factor for the deposited isotope composition, which is demonstrated by opposite δ^{98}Mo trends of shallow and deep sediments in the Guaymas OMZ (Eroglu et al., 2020 and this study) and the southern Peruvian margin. Figure modified from Eroglu et al. (2020). (B) Molybdenum concentration ranges in different sulfidic settings (Scott and Lyons, 2012) and variable Mo_{auth} content of shallow and deep sediments in the Guaymas OMZ (Eroglu et al., 2020 and this study) and the southern Peruvian margin.

2. Methods

2.1. Sampling procedure and porewater analyses

Sediment sampling was performed following the descriptions of Scholz et al. (2011). Cores were taken by a multicorer device (MUC) and cut into 1-4 cm slices. Shallow samples taken from the Guaymas slope (MUC09) were plugged immediately after recovery and further treated in a cooled lab at approximate seafloor temperature. Gravity cores were deployed with PVC liners. Upon recovery, the liners were cut into 1 m segments and the pore water was recovered using rhizons. Following pore water extraction, the liners were split lengthwise and sediment samples were taken with cut-off syringes. Hydrogen sulfide concentrations in pore water were determined after filtration (<0.2 µm pore size) by standard spectrophotometric techniques (Cline, 1969; Stookey, 1970). Fe concentrations were measured via inductively coupled plasma optical emission spectrometry (ICP-OES, Varian 720-ES) at GEOMAR in Kiel. Reproducibility and data quality was checked regularly using IAPSO as seawater reference.

2.1. Major and trace element analyses

Sediment samples were freeze-dried, powdered with an agate mill, and weighed into PFE vials. About 100 mg of sediment per sample was digested in a HF-HNO_3-$HClO_4$ acid mixture, and placed on a hotplate at 185°C for 24 hours. Digested samples were subsequently evaporated, re-dissolved in concentrated HNO_3, placed on a hotplate at 130°C for 24 hours, again evaporated and finally re-dissolved in diluted HNO_3. Major and trace element concentrations of dissolved sediment samples were

determined via inductively coupled plasma optical emission spectrometry (ICP-OES, Varian 720-ES) and mass spectrometry (ICP-MS, Agilent Technologies 7500 Series) analyses. External reproducibility of reference standards SDO-1 (Devonian Ohio Shale, USGS), MESS-3 (Marine Sediment Reference Material, Canadian Research Council), PACS-3 (Marine Sediment Reference Material, Canadian Research Council), and BHVO-1 (Basalt, Hawaiian Volcanic Observatory, USGS) was <1% (RSD) for Al, and Fe and <5% (RSD) for Mo.

2.2 TOC

Total organic carbon (TOC) analyses of sediment samples were determined by flash combustion in a Carlo-Erba Element Analyzer (NA1500) and analytical precision for replicate analyses was about 1% (RSD).

2.2. Fe speciation analyses

Sequential extractions of highly reactive Fe phases were applied on sediment powders following Poulton and Canfield (2005) and Canfield et al. (1986). In brief, (1) sodium acetate was used to extract Fe-carbonate and –monosulfide (Fe_{carb}), (2) sodium dithionite was used to extract Fe oxides (Fe_{ox}), (3) ammonium oxalate was used to extract magnetite (Fe_{mag}), and (4) a chromium chloride distillation was used to determine pyrite Fe (Fe_{Py}). Extraction solutions were measured for Fe concentrations by ICP-OES and sulfur concentrations in pyrite were determined by photometry and converted to Fe concentrations by assuming a Fe to sulfur stoichiometry of 1:2. The accuracy and precision of the method was determined by extracting and measuring standards that were calibrated in the framework of an interlaboratory comparison (Alcott et al., 2020). The sum of all four fractions is referred to as highly reactive Fe (Fe_{HR}). Any remaining Fe represents poorly reactive and unreactive silicate Fe.

2.3. Mo isotope analyses

The Mo purification procedure is based on the protocols of Siebert et al. (2001), Voegelin et al. (2009) and Wille et al. (2007). Prior to chemical separation, we added an adequate amount of ^{100}Mo-^{97}Mo double spike to the sediment and pore water samples in order to correct for any isotope fractionation during laboratory treatment and instrumental mass bias. Molybdenum was separated from the matrix and mass-interfering elements via ion exchange column chemistry using a column filled with 2 ml Biorad AG50W-X8 cation resin and washing and eluting with 0.5 M HCl, followed by a column filled with 1 ml Biorad AG1-X8 anion resin, washing with 4 M HCl and eluting with 2 M HNO_3. Yields after column chemistry were typically >90 % and procedural blanks were < 2 ng Mo which contributes less than 1% of total Mo.

Isotope analyses were carried out on a Nu Plasma MC-ICP-MS at the Isotope Geochemistry Labs at GEOMAR. Samples were introduced to the plasma ion source via a DSN-100 desolvating nebulizer system with an uptake rate of ~70 µl/min. Solutions had concentrations between 40 to 50 ng/ml and

were measured at a signal of about 700 mV on ^{96}Mo using a 10^{11} Ω resistor. We measured sediment samples in 4 blocks of 10 cycles per sample with a 10 s signal integration time each.

Sample δ^{98}Mo values were measured relative to the Alfa Aesar Mo standard solution, Specpure #38791 (lot no. 011895D) and a long-term external reproducibility of ± 0.07 ‰ (2SD, n = 201) was achieved. The international standard NIST-SRM-3134 was also measured repeatedly during each measurement session and is offset from the Alfa Aesar standard by +0.15 ± 0.08 ‰ (2SD, n = 46), which is in agreement with published values of Greber et al. (2012) and Nägler et al. (2014). Following Nägler et al. (2014), we present the results in the δ-notation relative to NIST-SRM-3134 with an offset of +0.25 ‰ and expressed in permil [‰]:

$$\delta^{98}Mo\ [‰] = \left[\frac{^{98}Mo/^{95}Mo_{sample}}{^{98}Mo/^{95}Mo_{NIST-SRM-3134}} - 1\right] \times 1000 + 0.25$$

In order to determine a realistic long term reproducibility of a matrix sample, USGS rock reference material SDO-1 (Devonian Ohio Shale) was chemically processed and analyzed with each batch of samples. The external reproducibility is +1.03 ± 0.09 ‰ (2SD, n = 43), which is in agreement with values of Goldberg et al. (2013) and references therein. Reported authigenic δ^{98}Mo data ($\delta^{98}Mo_{auth}$) are calculated from the authigenic fraction (Mo_{auth}), assuming that the lithogenic Mo fraction has an average isotope composition of +0.2 ‰ ($\delta^{98}Mo_{UCC}$) (Willbold and Elliott, 2017):

$$\delta^{98}Mo_{auth} = \frac{\delta^{98}Mo_{total} - \left(\left(1 - \frac{Mo_{auth}}{Mo_{total}}\right) \times \left(\delta^{98}Mo_{UCC}\right)\right)}{\frac{Mo_{auth}}{Mo_{total}}}$$

3. Tables

Table 1: Sulfate and hydrogen sulfide concentrations of porewater samples of deep sediments from the Guaymas slope (Gulf of California) taken during cruise SO241

Guaymas slope (676 m water depth)		
Deep sediments (SO241/47 GC7) [cm sediment depth]	SO_4^{2-} (mM)	H_2S (mM)
5	26.0	0.0
10	26.7	0.0
12	26.4	0.0
15	26.2	0.0
20	24.7	0.3
25	24.3	0.3
30	24.1	0.3
35	23.5	0.4
40	22.6	0.5
45	22.6	0.6
50	23.8	0.8
60	21.0	0.9
70	20.8	1.1
80	19.9	1.2
90	19.0	1.4
100	18.4	1.5
140	18.4	1.9
160	17.0	2.4
180	14.8	2.6
200	13.0	2.9
230	12.0	3.4
260	10.1	4.0
290	5.1	4.4
320	2.8	5.1
350	1.0	5.2
380	0.7	5.3
410	0.7	5.0
440	0.7	4.8
470	0.7	4.5
500	0.6	4.9
530	0.6	4.5
560	0.6	4.3
590	0.6	3.9
620	0.5	3.5
650	0.6	2.9
680	0.5	2.6
710	0.5	2.2
740	0.4	2.1

Table 2: Fe speciation ratios, Mo content and isotope composition, and total organic carbon content of the shallow (Eroglu et al., 2020) and deep sediments (this study) from the Guaymas slope (Gulf of California)

Guaymas slope (676 m water depth)	**27.71 °N 111.23 °W**												
Shallow sediments (SO241/29 MUC09) [cm sediment depth]		Fe_{carb}	Fe_{ox}	Fe_{mag}	Fe_{Py}	Fe_T	Fe_U	Fe_{Py}/Fe_{HR}	Fe_{HR}/Fe_T	Fe_T/Al	Mo_{auth} ($\mu g\ g^{-1}$)	$\delta^{98}Mo_{auth}$ (‰)	TOC (wt-%)
0.5		0.12	0.27	0.03	0.07	1.73	1.25	0.15	0.28	0.49	3.5	1.99	2.79
1.5		0.19	0.48	0.06	0.07	2.24	1.44	0.09	0.36	0.48	4.5	2.07	3.12
2.5		0.14	0.47	0.05	0.08	2.28	1.55	0.11	0.32	0.47	4.2	2.03	3.25
3.5		0.18	0.47	0.05	0.06	2.27	1.51	0.08	0.34	0.48	4.4	1.98	3.24
4.5		0.17	0.48	0.07	0.08	2.33	1.53	0.09	0.34	0.48	3.8	2.00	3.37
5.5		0.14	0.49	0.07	0.08	2.43	1.65	0.11	0.32	0.48	3.8	2.00	3.52
6.5		0.11	0.49	0.05	0.06	2.38	1.67	0.08	0.30	0.47	4.1	2.12	3.50
7.5		0.11	0.51	0.06	0.09	2.50	1.73	0.12	0.31	0.47	7.4	2.13	3.37
9		0.08	0.47	0.06	0.08	2.39	1.70	0.11	0.29	0.46	5.4	2.05	3.31
11		0.08	0.45	0.06	0.07	1.66	0.99	0.11	0.40	0.42	6.0	2.05	3.40
13		0.06	0.42	0.05	0.07	2.20	1.59	0.12	0.28	0.45	17.2	2.13	3.48
15		0.07	0.45	0.06	0.03	2.42	1.80	0.05	0.25	0.45	3.4	1.64	3.40
17.5		0.07	0.47	0.05	0.13	2.45	1.72	0.18	0.30	0.45	3.3	1.69	3.33
20.5		0.07	0.44	0.05	0.18	2.46	1.72	0.24	0.30	0.46	5.1	1.65	3.52
23.5		0.08	0.43	0.05	0.17	2.53	1.80	0.23	0.29	0.45	3.8	1.90	3.09
26.5		0.08	0.35	0.06	0.17	2.16	1.49	0.26	0.31	0.45	4.7	1.90	3.37
30		0.15	0.26	0.04	0.45	2.13	1.24	0.50	0.42	0.51	8.5	1.78	3.46
34		0.10	0.24	0.04	0.31	2.14	1.45	0.45	0.32	0.47	5.8	1.82	3.22
38		0.10	0.21	0.04	0.34	2.02	1.33	0.50	0.34	0.44	7.4	1.80	3.33
Deep sediments (SO241/47 GC7) [cm sediment depth]	years BP	Fe_{carb}	Fe_{ox}	Fe_{mag}	Fe_{Py}	Fe_T	Fe_U	Fe_{Py}/Fe_{HR}	Fe_{HR}/Fe_T	Fe_T/Al	Mo_{auth} ($\mu g\ g^{-1}$)	$\delta^{98}Mo_{auth}$ (‰)	TOC (wt-%)
5	197									0.46	5.2	1.69	2.77
25	265									0.45	7.4	1.82	3.13
50	358	0.15	0.20	0.06	0.44	2.05	1.20	0.52	0.42	0.45	6.8	1.67	3.62
90	527									0.46	8.8	1.67	3.41
130	720	0.24	0.21	0.07	0.67	2.48	1.28	0.56	0.48	0.47	4.6	1.84	3.13
170	937									0.47	5.2	1.72	3.3
210	1178	0.25	0.20	0.07	0.82	2.58	1.24	0.61	0.52	0.46	7.3	1.66	3.43
250	1442									0.46	6.4	1.68	3.25
290	1731	0.18	0.17	0.07	0.84	2.48	1.22	0.66	0.51	0.46	7.2	1.67	3.56
330	2044	0.23	0.17	0.06	0.56	2.27	1.25	0.55	0.45	0.44	6.4	1.71	3.19
368	2363	0.24	0.18	0.06	0.76	2.37	1.13	0.61	0.52	0.48	6.7	1.76	3.4
408	2723	0.26	0.16	0.06	0.66	2.25	1.11	0.58	0.51	0.44	7.2	1.68	3.01
448	3106									0.46	5.2	1.71	2.85
488	3514	0.27	0.22	0.07	0.66	2.49	1.28	0.54	0.49	0.45	5.7	1.81	3.32
528	3946									0.45	4.3	1.79	2.92
568	4695	0.29	0.19	0.08	0.68	2.57	1.33	0.55	0.48	0.44	6.3	1.8	3.33
608	5813									0.43	5.7	1.83	3.06
648	6931	0.27	0.20	0.08	0.72	2.66	1.40	0.57	0.47	0.44	4.7	1.92	3.18
688	8049									0.43	4.1	1.75	2.73
728	9167	0.29	0.20	0.07	0.67	2.70	1.47	0.54	0.46	0.41	3.6	1.89	2.78
763	10145									0.42	5.2	1.77	2.69

BP: before present; Fe_{carb}: carbonate-associated iron; Fe_{ox}: reducible iron (oxyhydr)oxides; Fe_{mag}: magnetite iron; Fe_T: total iron; Fe_U: poorly reactive and unreactive iron (Fe_T-(Fe_{carb}+Fe_{ox}+Fe_{mag}+Fe_{Py}))

Table 3: Fe speciation ratios, Mo content and isotope composition, and total organic carbon content of the shallow and deep sediments (this study; ages from Salvatteci et al., 2019) off southern Peru

Southern Peruvian OMZ	**17.25 °S**												
(232 m water depth)	**71.44 °W**												
Shallow sediments (M135-004-2) [cm sediment depth]		Fe_{carb}	Fe_{ox}	Fe_{mag}	Fe_{Py}	Fe_T	Fe_U	Fe_{Py}/Fe_{HR}	Fe_{HR}/Fe_T	Fe_T/Al	Mo_{auth} (µg g^{-1})	$\delta^{98}Mo_{auth}$ (‰)	TOC (wt-%)
0.5		0.10	0.42	0.12	0.09	2.79	2.06	0.13	0.26	0.42	9.0	1.30	3.72
1.5										0.42	7.1		3.50
2.5		0.08	0.55	0.12	0.06	3.01	2.20	0.07	0.27	0.43	6.2	1.29	2.70
3.5										0.41	8.3		4.27
4.5		0.06	0.47	0.11	0.08	2.81	2.10	0.12	0.26	0.40	10.5	1.29	4.54
5.5										0.41	11.3		5.09
6.5										0.40	10.6		3.77
7.5										0.40	9.3		3.27
8.5										0.42	10.1		3.24
9.5										0.44	9.2		2.99
11.5		0.12	0.53	0.14	0.10	3.26	2.37	0.11	0.27	0.44	8.9	1.17	2.66
14.5		0.17	0.45	0.11	0.22	3.05	2.09	0.23	0.31	0.45	13.1	1.28	3.96
16.5										0.42	11.8		4.30
18.5										0.42	11.7		5.05
23.5		0.06	0.31	0.11	0.09	2.87	2.30	0.17	0.20	0.39	8.9	1.35	4.08
28.5		0.08	0.25	0.09	0.18	2.77	2.16	0.30	0.22	0.39	17.0	1.25	5.02
33.5		0.09	0.21	0.10	0.16	2.90	2.34	0.28	0.19	0.38	7.6	1.22	2.12
38.5										0.40	6.5		3.14
43.5										0.39	7.8		3.48
48.5										0.40	8.4		3.00
Deep sediments (M135-004-3) [cm sediment depth]	years BP	Fe_{carb}	Fe_{ox}	Fe_{mag}	Fe_{Py}	Fe_T	Fe_U	Fe_{Py}/Fe_{HR}	Fe_{HR}/Fe_T	Fe_T/Al	Mo_{auth} (µg g^{-1})	$\delta^{98}Mo_{auth}$ (‰)	TOC (wt-%)
8	141									0.38	5.9	1.42	2.25
18	183									0.38	6.5	1.44	2.78
38	444									0.41	7.8	1.40	1.91
53	640	0.29	0.11	0.06	0.69	2.78	1.64	0.60	0.41	0.35	2.3	1.23	0.90
78	966									0.44	17.0	1.25	4.61
88	1096	0.21	0.14	0.06	0.87	3.09	1.82	0.68	0.41	0.41	14.6	1.38	4.02
118	1488									0.39	12.0	1.45	3.70
153	1944	0.12	0.14	0.06	0.99	2.79	1.48	0.75	0.47	0.41	35.5	1.39	7.09
163	2075	0.10	0.13	0.08	0.90	2.75	1.55	0.75	0.44	0.40	31.5	1.53	6.67
196	2466	0.13	0.12	0.07	0.88	2.86	1.66	0.73	0.42	0.39	17.0	1.40	4.41
208	2662									0.39	14.9	1.47	4.61
228	2923									0.42	14.2	1.43	4.70
238	3053									0.41	8.5	1.41	3.08
258	3308	0.18	0.10	0.06	0.79	3.00	1.86	0.70	0.38	0.41	15.1	1.39	3.63
263	3373									0.38	15.8	1.31	4.15
288	3699									0.38	19.4	1.43	7.16
303	3895									0.39	21.1	1.43	6.42
318	4091	0.11	0.13	0.07	0.90	2.87	1.66	0.75	0.42	0.41	20.5	1.42	7.15
338	4352									0.41	15.1	1.32	4.08
348	4489									0.39	16.4	1.41	4.69
378	4880									0.40	12.0	1.23	3.71
388	5010	0.11	0.14	0.06	0.91	2.75	1.53	0.74	0.44	0.40	23.4	1.29	6.99
403	5206									0.40	18.2	1.39	5.16

Table 3 continued

[cm sediment depth]	years BP	Fe_{carb}	Fe_{ox}	Fe_{mag}	Fe_{Py}	Fe_T	Fe_U	Fe_{Py}/Fe_{HR}	Fe_{HR}/Fe_T	Fe_T/Al	Mo_{auth} ($\mu g\ g^{-1}$)	$\delta^{98}Mo_{auth}$ (‰)	TOC (wt-%)
433													
443	5728									0.40	19.0	1.26	4.04
468	6048	0.13	0.12	0.06	0.94	2.75	1.50	0.76	0.45	0.40	22.1	1.31	6.48
478	6178									0.42	18.1		5.08
508	6570									0.40	21.9	1.35	7.45
538	6961									0.43	15.0	1.46	3.99
558	7222	0.22	0.13	0.06	0.77	2.87	1.70	0.66	0.41	0.40	16.4	1.38	4.75
563	7287									0.42	17.3	1.37	5.33
583	7548									0.40	23.3	1.35	6.69
598	7744									0.44	18.0	1.39	3.62
608	7874									0.43	14.7	1.42	4.74
618	8005									0.42	16.7	1.47	4.69
633	8200	0.12	0.12	0.06	0.78	3.02	1.94	0.72	0.36	0.43	19.2	1.30	5.42
638	8266									0.41	17.9	1.33	4.14
663	8592									0.43	26.1	1.42	6.18
698	9049									0.41	12.0	1.45	3.49
718	9309									0.40	15.8	1.36	3.69

BP: before present; Fe_{carb}: carbonate-associated iron; Fe_{ox}: reducible iron (oxyhydr)oxides; Fe_{mag}: magnetite iron; Fe_T: total iron; Fe_U: poorly reactive and unreactive iron (Fe_T-(Fe_{carb}+Fe_{ox}+Fe_{mag}+Fe_{Py}))

REFERENCES

Alcott, L. J., Krause, A. J., Hammarlund, E. U., Bjerrum, C. J., Scholz, F., Xiong, Y. J., Hobson, A. J., Neve, L., Mills, B. J. W., Marz, C., Schnetger, B., Bekker, A., and Poulton, S. W., 2020, Development of Iron Speciation Reference Materials for Palaeoredox Analysis: Geostandards and Geoanalytical Research, v. 44, no. 3, p. 581-591.

Anderson, T. F., and Raiswell, R., 2004, Sources and mechanisms for the enrichment of highly reactive iron in euxinic Black Sea sediments: American Journal of Science, v. 304, no. 3, p. 203-233.

Arnold, G. L., Anbar, A. D., Barling, J., and Lyons, T. W., 2004, Molybdenum isotope evidence for widespread anoxia in mid-proterozoic oceans: Science, v. 304, no. 5667, p. 87-90.

Barling, J., Arnold, G. L., and Anbar, A. D., 2001, Natural mass-dependent variations in the isotopic composition of molybdenum: Earth and Planetary Science Letters, v. 193, no. 3-4, p. 447-457.

Berner, R. A., 1970, Sedimentary Pyrite Formation: American Journal of Science, v. 268, no. 1, p. 1-&.

Bostick, B. C., Fendorf, S., and Helz, G. R., 2003, Differential adsorption of molybdate and tetrathiomolybdate on pyrite (FeS2): Environmental Science & Technology, v. 37, no. 2, p. 285-291.

Canfield, D. E., Poulton, S. W., Knoll, A. H., Narbonne, G. M., Ross, G., Goldberg, T., and Strauss, H., 2008, Ferruginous conditions dominated later neoproterozoic deep-water chemistry: Science, v. 321, no. 5891, p. 949-952.

Canfield, D. E., Raiswell, R., Westrich, J. T., Reaves, C. M., and Berner, R. A., 1986, The Use of Chromium Reduction in the Analysis of Reduced Inorganic Sulfur in Sediments and Shales: Chemical Geology, v. 54, no. 1-2, p. 149-155.

Chappaz, A., Lyons, T. W., Gregory, D. D., Reinhard, C. T., Gill, B. C., Li, C., and Large, R. R., 2014, Does pyrite act as an important host for molybdenum in modern and ancient euxinic sediments?: Geochimica Et Cosmochimica Acta, v. 126, p. 112-122.

Cline, J. D., 1969, Spectrophotometric Determination of Hydrogen Sulfide in Natural Waters: Limnology and Oceanography, v. 14, no. 3, p. 454-&.

Dahl, T. W., Chappaz, A., Hoek, J., McKenzie, C. J., Svane, S., and Canfield, D. E., 2017, Evidence of molybdenum association with particulate organic matter under sulfidic conditions: Geobiology, v. 15, no. 2, p. 311-323.

Dellwig, O., Bottcher, M. E., Lipinski, M., and Brumsack, H. J., 2002, Trace metals in Holocene coastal peats and their relation to pyrite formation (NW Germany): Chemical Geology, v. 182, no. 2-4, p. 423-442.

Eroglu, S., Scholz, F., Frank, M., and Siebert, C., 2020, Influence of particulate versus diffusive molybdenum supply mechanisms on the molybdenum isotope composition of continental margin sediments: Geochimica Et Cosmochimica Acta, v. 273, p. 51-69.

Goldberg, T., Gordon, G., Izon, G., Archer, C., Pearce, C. R., McManus, J., Anbar, A. D., and Rehkamper, M., 2013, Resolution of inter-laboratory discrepancies in Mo isotope data: an intercalibration: Journal of Analytical Atomic Spectrometry, v. 28, no. 5, p. 724-735.

Greber, N. D., Siebert, C., Nagler, T. F., and Pettke, T., 2012, d98/95Mo values and Molybdenum Concentration Data for NIST SRM 610, 612 and 3134: Towards a Common Protocol for Reporting Mo Data: Geostandards and Geoanalytical Research, v. 36, no. 3, p. 291-300.

Helz, G. R., Erickson, B. E., and Vorlicek, T. P., 2014, Stabilities of thiomolybdate complexes of iron; implications for retention of essential trace elements (Fe, Cu, Mo) in sulfidic waters: Metallomics, v. 6, no. 6, p. 1131-1140.

Helz, G. R., Miller, C. V., Charnock, J. M., Mosselmans, J. F. W., Pattrick, R. A. D., Garner, C. D., and Vaughan, D. J., 1996, Mechanism of molybdenum removal from the sea and its concentration in black shales: EXAFS evidence: Geochimica Et Cosmochimica Acta, v. 60, no. 19, p. 3631-3642.

Huerta-Diaz, M. A., and Morse, J. W., 1992, Pyritization of Trace-Metals in Anoxic Marine-Sediments: Geochimica Et Cosmochimica Acta, v. 56, no. 7, p. 2681-2702.

Lyons, T. W., and Severmann, S., 2006, A critical look at iron paleoredox proxies: New insights from modern euxinic marine basins: Geochimica Et Cosmochimica Acta, v. 70, no. 23, p. 5698-5722.

Lyons, T. W., Werne, J. P., Hollander, D. J., and Murray, R. W., 2003, Contrasting sulfur geochemistry and Fe/Al and Mo/Al ratios across the last oxic-to-anoxic transition in the Cariaco Basin, Venezuela: Chemical Geology, v. 195, no. 1-4, p. 131-157.

März, C., Poulton, S. W., Beckmann, B., Kuster, K., Wagner, T., and Kasten, S., 2008, Redox sensitivity of P cycling during marine black shale formation: Dynamics of sulfidic and anoxic, non-sulfidic bottom waters: Geochimica Et Cosmochimica Acta, v. 72, no. 15, p. 3703-3717.

McManus, J., Berelson, W. M., Severmann, S., Poulson, R. L., Hammond, D. E., Klinkhammer, G. P., and Holm, C., 2006, Molybdenum and uranium geochemistry in continental margin sediments: Paleoproxy potential: Geochimica Et Cosmochimica Acta, v. 70, no. 18, p. 4643-4662.

Nägler, T. F., Anbar, A. D., Archer, C., Goldberg, T., Gordon, G. W., Greber, N. D., Siebert, C., Sohrin, Y., and Vance, D., 2014, Proposal for an International Molybdenum Isotope Measurement Standard and Data Representation: Geostandards and Geoanalytical Research, v. 38, no. 2, p. 149-151.

Poulson-Brucker, R. L. P., McManus, J., and Poulton, S. W., 2012, Molybdenum isotope fractionations observed under anoxic experimental conditions: Geochemical Journal, v. 46, no. 3, p. 201-209.

Poulson-Brucker, R. L. P., McManus, J., Severmann, S., and Berelson, W. M., 2009, Molybdenum behavior during early diagenesis: Insights from Mo isotopes: Geochemistry Geophysics Geosystems, v. 10.

Poulson, R. L., Siebert, C., McManus, J., and Berelson, W. M., 2006, Authigenic molybdenum isotope signatures in marine sediments: Geology, v. 34, no. 8, p. 617-620.

Poulton, S. W., and Canfield, D. E., 2005, Development of a sequential extraction procedure for iron: implications for iron partitioning in continentally derived particulates: Chemical Geology, v. 214, no. 3-4, p. 209-221.

-, 2011, Ferruginous Conditions: A Dominant Feature of the Ocean through Earth's History: Elements, v. 7, no. 2, p. 107-112.

Poulton, S. W., Krom, M. D., and Raiswell, R., 2004, A revised scheme for the reactivity of iron (oxyhydr)oxide minerals towards dissolved sulfide: Geochimica Et Cosmochimica Acta, v. 68, no. 18, p. 3703-3715.

Raiswell, R., and Canfield, D. E., 1998, Sources of iron for pyrite formation in marine sediments: American Journal of Science, v. 298, no. 3, p. 219-245.

Raiswell, R., Hardisty, D. S., Lyons, T. W., Canfield, D. E., Owens, J. D., Planavsky, N. J., Poulton, S. W., and Reinhard, C. T., 2018, The Iron Paleoredox Proxies: A Guide to the Pitfalls, Problems and Proper Practice: American Journal of Science, v. 318, no. 5, p. 491-526.

Raiswell, R., Newton, R., and Wignall, P. B., 2001, An indicator of water-column anoxia: Resolution of biofacies variations in the Kimmeridge Clay (Upper Jurassic, UK): Journal of Sedimentary Research, v. 71, no. 2, p. 286-294.

Raiswell, R., and Plant, J., 1980, The Incorporation of Trace-Elements into Pyrite during Diagenesis of Black Shales, Yorkshire, England: Economic Geology, v. 75, no. 5, p. 684-699.

Scholz, F., 2018, Identifying oxygen minimum zone-type biogeochemical cycling in Earth history using inorganic geochemical proxies: Earth-Science Reviews, v. 184, p. 29-45.

Scholz, F., Hensen, C., Noffke, A., Rohde, A., Liebetrau, V., and Wallmann, K., 2011, Early diagenesis of redox-sensitive trace metals in the Peru upwelling area - response to ENSO-related oxygen fluctuations in the water column: Geochimica Et Cosmochimica Acta, v. 75, no. 22, p. 7257-7276.

Scott, C., and Lyons, T. W., 2012, Contrasting molybdenum cycling and isotopic properties in euxinic versus non-euxinic sediments and sedimentary rocks: Refining the paleoproxies: Chemical Geology, v. 324, p. 19-27.

Siebert, C., McManus, J., Bice, A., Poulson, R., and Berelson, W. M., 2006, Molybdenum isotope signatures in continental margin marine sediments: Earth and Planetary Science Letters, v. 241, no. 3-4, p. 723-733.

Siebert, C., Nagler, T. F., and Kramers, J. D., 2001, Determination of molybdenum isotope fractionation by double-spike multicollector inductively coupled plasma mass spectrometry: Geochemistry Geophysics Geosystems, v. 2, p. art. no.-2000GC000124.

Siebert, C., Nagler, T. F., von Blanckenburg, F., and Kramers, J. D., 2003, Molybdenum isotope records as a potential new proxy for paleoceanography: Earth and Planetary Science Letters, v. 211, no. 1-2, p. 159-171.

Stookey, L. L., 1970, Ferrozine - a New Spectrophotometric Reagent for Iron: Analytical Chemistry, v. 42, no. 7, p. 779-&.

Tribovillard, N., Riboulleau, A., Lyons, T., and Baudin, F. O., 2004, Enhanced trapping of molybdenum by sulfurized marine organic matter of marine origin in Mesozoic limestones and shales: Chemical Geology, v. 213, no. 4, p. 385-401.

Voegelin, A. R., Nagler, T. F., Samankassou, E., and Villa, I. M., 2009, Molybdenum isotopic composition of modern and Carboniferous carbonates: Chemical Geology, v. 265, no. 3-4, p. 488-498.

Wagner, M., Chappaz, A., and Lyons, T. W., 2017, Molybdenum speciation and burial pathway in weakly sulfidic environments: Insights from XAFS: Geochimica Et Cosmochimica Acta, v. 206, p. 18-29.

Willbold, M., and Elliott, T., 2017, Molybdenum isotope variations in magmatic rocks: Chemical Geology, v. 449, p. 253-268.

Wille, M., Kramers, J. D., Nagler, T. F., Beukes, N. J., Schroder, S., Meisel, T., Lacassie, J. P., and Voegelin, A. R., 2007, Evidence for a gradual rise of oxygen between 2.6 and 2.5 Ga from Mo isotopes and Re-PGE signatures in shales: Geochimica Et Cosmochimica Acta, v. 71, no. 10, p. 2417-2435.